Open access • Journal Article • DOI:10.13182/FST86-A24718

Low temperature plasma near a tokamak reactor limiter — Source link

Bastiaan J. Braams, Clifford E. Singer

Institutions: Princeton Plasma Physics Laboratory

Published on: 01 Mar 1986 - Fusion Technology (American Nuclear Society)

Topics: Limiter, Tokamak, Fusion power and Plasma parameters

PPPL-2191 (1)

DR-0794-3 I-19353 PPPL-2191

UC20-A,C,D,G

LOW TEMPERATURE PLASMA NEAR A TOKAMAK REACTOR LIMITER

By

B.J. Braams and C.E. Singer

JANUARY 1985

PLASMA PHYSICS LABORATORY

PRINCETON UNIVERSITY
PRINCETON, NEW JERSEY

PREPARED FOR THE U.S. DEPARTMENT OF ENERGY,
UNDER CONTRACT DE-AC02-76-CHO-3073.

PPPL--2191

DE85 007138

LOW TEMPERATURE PLASMA NEAR A TOKAMAK REACTOR LIMITER

B. J. Braams* and C. E. Singer

Plasma Physics Laboratory, Princeton University

Princeton, New Jersey 08544

ABSTRACT

Analytic and two-dimensional computational solutions for the plasma parameters near a toroidally symmetric limiter are illustrated for the projected parameters of a Tokamak Fusion Core Experiment (TFCX). The temperature near the limiter plate is below 20 eV, except when the density 10 cm inside the limiter contact is $8 \times 10^{13} cm^{-3}$ or less and the thermal diffusivity in the edge region is $2 \times 10^{4} cm^{2}/s$ or less. Extrapolation of recent experimental data suggests that neither of these conditions is likely to be met near ignition in TFCX, so a low plasma temperature near the limiter should be considered a likely possibility.

*F.O.M. Instituut voor Plasmafysica, Nieuwegein, The Netherlands.

I. INTRODUCTION

In order to have an adequate safety margin against sputtering and erosion, the plasma near a material boundary in a tokamak should have an electron temperature of about 10 eV or less. This is relatively easy to achieve with an expanded boundary or divertor configuration,[1] where the large volume in the boundary allows the possibility of radiating a significant power. A large scrape-off thickness can be achieved by radial neoclassical and/or charge-exchange transport because the competing process of heat conduction parallel to the magnetic field occurs over an extended connection length near the magnetic separatrix.

The requirements for achieving low temperature near a limiter plate have not been well defined. Earlier work used poloidally averaged transport models to investigate "cold plasma mantel" solutions to this problem.[2] These solutions required a sizeable poloidally averaged impurity density on the outermost flux surfaces in order to radiate the power flow from an ignited (or nearly ignited) plasma core. This required limited inward plasma transport near the plasma periphery in order to avoid mixing impurities into the plasma core. Subsequent investigations of microinstabilities due to the strong radial temperature gradients have cast doubt on whether such a cold plasma mantle can be obtained in practice.[3]

Recent experience has shown that poloidal asymmetries play a dominant role in the energy flows in the peripheral plasma in a tokamak. We have therefore reinvestigated the question of tokamak boundary conditions by including consideration of poloidal asymmetries in an analysis of the temperature expected near the limiter of a tokamak with an ignited plasma core. First, we adapt a simple "two-point model" of the poloidal asymmetries[4] in order to illustrate the important contributions to the energy and particle flows. Then we present numerical solutions of two-dimensional particle, momentum, and energy balances.

The emphasis here is not on working out in great detail the consequences of a specific set of assumptions about boundary density, radial transport coefficients, etc. Rather, we survey a variety of assumptions to see which give an acceptable temperature near the limiter plate. We then go on to review briefly the present state of knowledge about energy and particle transport, and we argue that favorable solutions are reasonably likely to be realized in practice. This has significant implications for the range of options which must be considered in designing limiters for ignition experiments.

II. TWO-POINT MODEL

The geometry of the two-point model[4,5] is shown in Fig. 1. For the particular example worked out here, the limiter is positioned at the bottom, but the diagram can be rotated ±90% for inboard or outboard limiters. The power from the plasma core is assumed to leave the upper scrape-off regions by heat conduction along magnetic field lines. The D-shaped toroidal plasma is first modeled as an equivalent-circular cylinder and the scrape-off regions are then elongated to rectangular boxes. Half of the power flows through each of two such boxes, only one of which is shown here and modeled below. The width of the scrape-off region is taken as twice the half-width L_ψ estimated from the power balance for the first region,

$$\frac{n\chi T A_{core}}{L_\psi} = Q_{core} ,$$

n, χ, and T are the density, temperature, and radial thermal diffusivity in region 1, $A_{core} = 4\pi^2 R_o a_{eq}$ is the surface area of the plasma core (where R_o is the major radius, and a_{eq} is the circular equivalent minor radius), and Q_{core} is the power outflux from the core.

The energy balance for each of the scrape-off regions near the limiter in the analytic model includes conduction from region 1, radiative losses in region 2, and transport to the limiter through an electrostatic sheath

$$\frac{1}{2} Q_{core} = Q_{cond} = P_{rad} + Q_{sheath} ,$$

where

$$Q_{cond} = \frac{B_\theta}{B} q_\parallel A ,$$

$$q_\parallel = -\kappa \frac{T_2 - T_1}{L_\parallel} ,$$

$$\kappa = \left(\frac{\gamma_o}{Z_{eff}}\right) \frac{3T^{5/2}}{4\, m_e^{1/2}\, (2\pi)^{1/2} \lambda\, e^4} ,$$

$$T = \frac{T_1 + T_2}{2} ,$$

and where $\gamma_o = 12.2 - 9\, Z_{eff}^{-1/2}$ and λ are the non-Lorentz gas correction and Coulomb logarithm given by Braginskii.[6] (Note that we cannot conveniently integrate this energy balance[7] when there is a substantial contribution from radiation, so we have taken care to boundary-center the value of T used in computing the parallel conductivity.) We include carbon radiation

$$P_{rad} = n_2^2 f_c L_Z V_2 ,$$

where $f_c = (Z_{eff} - 1)/Z_c(Z_c + 1)$ relates the fractional carbon concentration to its mean charge, Z_c, and the effective charge, Z_{eff}, and $L_Z \approx 5 \times 10^{-19}$ erg cm^{-3} s^{-1} is the coronal equilibrium radiation rate for carbon near 10 eV.[8] The geometric parameters in the energy balance are the effective length $L_\parallel$ of the region 1, the area $A = 2\pi R_o \Delta$ of the boundary between the regions (with $\Delta = 2L_\psi$), the volume $V_2 = 2\pi R L_2 \Delta$ of region 2 where L_2 is the poloidal length of region 2, and the magnetic field inclination $B_\theta/B \approx \varepsilon/q$ where $\varepsilon = a_{eq}/R$ is the inverse aspect ratio and q is the equivalent circular safety factor. The energy flow to the sheath is $Q_{sheath} = 8nvT\, AB_\theta/B$ where $v < (2T/\bar{m}_i)^{1/2}$, $\bar{m}_i = \bar{A}_i m_p$, m_p is the proton mass, and $\bar{A}_i$ is the average ion atomic mass.

These equations allow one to determine the upstream temperature, T_1, as a function of downstream density n_2 and temperature T_2, given assumptions about Q_{core}, χ, Z_{eff}, and the geometric quantities $L_\parallel$, L_2, R, a_{eq}, and q. The upstream density is determined by assuming half the upstream pressure is lost to kinetic motion in the downstream region to obtain $n_1T_1 = 2n_2T_2$. It is also of interest to compute the ratio R of the plasma flux on the plate to the particle outflux from region 1:

$$R^{-1} = 1 - \left(1 - f_{leak}\right)\left(1 - e^{-\kappa_o}\right)$$

where

$$\kappa_o = L_o/\lambda^o_{mfp} ,$$

is the neutral opacity of region 2, $\lambda^o_{mfp} = v_o/(n_2 \langle\sigma v\rangle_2)$ is the neutral mean-free path, $v_o = [2E_o/(\bar{A}_o m_p)]^{1/2}$ is the neutral velocity, E_o is the neutral energy, $\bar{A}_o$ is the mean atomic mass of the neutrals, $\langle\sigma v\rangle_2$ is the electron impact ionization rate coefficient evaluated at the temperature T_2 (cf. Sec. III-A), $L_o = 2^{1/2} L_\phi$ is the effective path length for neutrals in region 2, and $f_{leak} = e^{-\kappa_o}$ is the transverse leakage of neutrals from the recycling region. (The peculiar notation here is adapted from treatments of divertor plasma where the transverse leakage and penetration through the recycling region are not identical.) The Mach number of the flow just before the recycling region is then

$$M = \frac{1}{2R} \left(\frac{T_1}{T_2}\right)^{1/2} .$$

A numerical example of the results of these equations, for $a_{eq} = 120 \times 1.6^{1/2} = 150$ cm, $R_o = 300$ cm, $Q_{core} = 50$ MW, $\chi = 5 \times 10^4 \mathrm{cm}^2/\mathrm{s}$, $E_o = T_2 = 12$ eV, $n_2 = 2 \times 10^{14} \mathrm{cm}^{-3}$, $L_2 = a_{eq}\pi/4 = 120$ cm, $q = 2.3$, $\bar{A}_1 = \bar{A}_o = 1.5$, $Z_c = 6$, and $Z_{eff} = 1.5$, gives $L_\phi = 1.4$ cm, $P_{rad} = 15$ MW, $Q_{sheath} = 10$ MW, $T_1 = 62$ eV, $n_1 = 0.8 \times 10^{14} \mathrm{cm}^{-3}$, $R = 2.0$ and $M = 0.56$. That is to say, reasonable upstream plasma conditions (n_1, T_1) appear to be compatible with reactor relevant power flux, low temperature near the limiter, and a moderately high recycling region preceded by subsonic flow. To test and elaborate the predictions of this simple model, two-dimensional transport simulations were performed.

III. TWO-DIMENSIONAL FLOWS

A. Fixed Parameters

The geometry described above was extended to include 10 cm of the plasma region on closed flux surfaces. The computational mesh is related to the corresponding TFCX geometry in Fig. 1. A typical result[9] is projected onto an MHD equilibrium for TFCX in Fig. 2. The transport equations were solved in rectangular geometry and included balances for electrons, momentum, electron energy, and ion energy, with classical bulk viscosity and parallel heat conduction and anomalous radial transport of particles, parallel momentum (i.e., anomalous shear viscosity), and ion and electron energy[7], as described in detail in the Appendix.[9,10] Viscous heating was also included in these calculations, but had no visually noticeable effect on graphs of the solutions. The radial ion thermal diffusivity and shear viscosity were $\chi_i = 0.2 \times 10^4 \mathrm{cm}^2/\mathrm{s}$ and $\eta_y^i = n\bar{A}_i m_p \chi_i$ where the mean ion mass number was $\bar{A}_i = 2.5$. (We denote the radial distance on the computational mesh by y and the poloidal distance by x.)

For this application, we employed a simple model of particle and energy sources based on exponential attenuation of recycling from the limiter and wall. Plasma striking the boundaries was recycled as 10 eV neutrals attenuated first along the field lines (for the limiter) and then radially inward. The attenuation of neutral flux through the plasma was computed from the rate of electron impact ionization. The ionization source rate coefficient was approximated by the expression $\langle\sigma v\rangle = 3 \times 10^{-8} \times a^2/(3 + a^2)$ $\mathrm{cm}^3\mathrm{s}^{-1}$, with $a = T_e/(10\ \mathrm{eV})$. Each ionization event removed 25 eV from the electron energy and added 5 eV to the ion energy.

Fixed boundary conditions at the outer wall were $n_i = 10^{13}\mathrm{cm}^{-3}$, $T_e = T_i = 2$ eV, $\partial u/\partial y = 0$, where u is the flow speed along the magnetic field. At the upstream end, we prescribed zero poloidal flow and zero poloidal gradients. At the downstream end inward from the limiter, zero flow and zero gradients were also prescribed; while on the limiter the conditions were $u = (p/\rho)^{1/2}$, and heat fluxes $Q_e = \delta_e n_e u T_e$, $Q_i = \delta_i n_i u T_i + 1/2\ \rho u^3$, with $\delta_e = 4$, $\delta_i = 5/2$, where $p = n(T_e + T_i)$ and $\rho = nm_p\bar{A}_i$. The conditions on the temperatures at the inner boundary were $T_e = T_i = T_m$, with T_m computed in the code in order to obtain an average power flux into the scrapeoff of 135 $\mathrm{kW/m}^2$. The parallel flow velocity was zero along the inner boundary.

B. Results of Parameter Variation

The radial energy and particle transport coefficients were varied, as was the density on the inner boundary. The energy and particle fluxes were

$$Q_j = -\chi_j n \frac{\partial T_j}{\partial y} \quad , j = e, i \, ,$$

$$\Gamma = -D \frac{\partial n}{\partial y} \quad .$$

χ_e was set to $2 \times 10^4 cm^2/s$ or $5 \times 10^4 cm^2/s$, with $D = \chi_e/2$ and $\chi_i = 2 \times 10^3 cm^2/s$.

Results of these parameter variations are given in Fig. 3 where we show the electron temperature in front of the limiter tip. For all but the lowest diffusivities and inner boundary densities, the temperature in front of the limiter is below 20 eV. Upstream from this location is a transition region (to use terminology used for a similar phenomenon in the solar atmosphere) to a point where electron heat conduction along field lines maintains nearly constant temperature. When the boundary density drops below a critical value, a cold recycling region fails to develop in front of the limiter, and the transition to low temperatures no longer occurs. The existence of such a critical density is compatible with the results of Petravic et al.[11] who predicted a maximum $T_e > 60$ eV near the TFCX limiter plate with an upstream core boundary density of $n_e = 0.4 \times 10^{14} cm^{-3}$. The critical density depends on radial transport. Enhanced radial transport dilutes the parallel heat flux density and facilitates formation of the temperature transition. When volumetric energy losses are included as here, then the sensitivity to radial transport rates is stronger than obtained from simpler analytic estimates. This is because increasing the volume of the scrape-off plasma soon leads to a situation where volume losses are significant, until the temperature in the recycling region becomes too low to support further volume losses.

Of particular interest is the poloidal power flow shown in Fig. 4. Peak poloidal flow is 8 MW/m^2, fading to 4 MW/m^2 in a radial distance of 1.6 cm.

C. Uncertainties in n_e and χ_e

To appreciate the significance of the above results requires an understanding of how scrape-off parameters have recently been chosen for reactor designs such as INTOR. To the best of our knowledge these parameters have been chosen as described below, first for the boundary density and then for the boundary diffusivity.

The boundary density is generally obtained from an estimated volume-average or peak core-plasma density and a ratio of the core-plasma density to the boundary value. The core/separatrix density ratio was found to be about three for a variety of conditions in the first studies of INTOR plasma parameters,[12] and later studies did not contradict this conclusion. However, we now know that very broad density profiles can develop in cases where intense edge-localized recycling can occur. One should therefore ask whether there is experimental evidence to support the expectation of peaked density profiles in ignited plasmas. It is true that many present tokamak experiments show peaked density profiles, but these experiments have substantial contributions from deep fueling profiles and/or the Ware pinch. By contrast, the present calculations show extremely shallow fueling profiles. The contribution of the Ware pinch in an ignition plasma is negligible, as shown by the flat central density profiles obtained with the Ware pinch included in early INTOR modeling studies. An assumption that ignition plasmas will have peaked density profiles must therefore be based on an extrapolation of an anomalous pinch. However, the evidence that an anomalous hydrogen pinch exists at all is based either on the dubious assumption of a flat or monotonic diffusion coefficient and/or a rather dubious analogy with impurity transport. There is therefore very little basis for extrapolating such an effect to ignited plasmas, as discussed elsewhere in detail.[13] To the extent that we have density profiles from high-power experiments with shallow fueling profiles, such as the PDX and ASDEX H-mode and possibly the PDX scoop experiment, the experimentally observed trend is toward very flat density profiles, with the density at 90% of the separatrix minor radius approaching one-half or more of the line-average density. These experiments still have an appreciable loop voltage and contribution from the Ware pinch. It therefore seems reasonable that we should investigate a case with relatively flat density profiles -- with the obvious qualification that all such extrapolations are difficult and other assumptions should be pursued in parallel. Using an extrapolation based on a purely empirical formula such as $\chi_e \sim 5 \times 10^{17}/n_e$ (INTOR) gives larger radial gradients at the boundary in one-dimensional radial transport simulations than have been observed in experiments. It seems dangerous to use such an empirical extrapolation of existing data which does not take account of the effect of such gradients. When one is forced to make an extrapolation of edge transport rates to construct a baseline case for point modeling studies, the best one can do is to use available extrapolations of the effect of gradients on transport. The only such model now available is a preliminary semiempirical model based on a very limited set of experimental simulations.[14] This model is consistent with the values at the radius of the limiter tip set to $\chi_e = 2D = 5 \times 10^4$ cm^2/s, as used to obtain the results described in Fig. 3.

According to the considerations given above, the value $n_e = 10^{14}$ cm^{-3} used here could conceivably be a rather low value for the inner boundary density, but a higher boundary density leads only to a proportionally higher density near the limiter plate with no qualitative difference in the patterns of temperature distribution, Mach number, or power flows. A higher χ_e is not necessary for achieving low T_e near the limiter in this density range.

IV. CONCLUSIONS

We have demonstrated solutions of two-dimensional plasma flows with low temperature and intense recycling near a limiter plate, and have explained why these solutions may be compatible with presently possible extrapolation from the limited existing experimental data. We have also investigated the dependence of these solutions on edge plasma transport, and shown that low temperature solutions occur under a variety of conditions. Of course, there are many other uncertainties about edge plasma. As one example, we set $\Gamma = -(\chi_e/3)\partial n/\partial y - (\chi_e/6)(n/p)(\partial p/\partial y)$ and got virtually identical results for Fig. 3 as with $\Gamma = -(\chi_e/2)\partial n/\partial y$. There are also significant problems with our neutral transport model which can only be rectified by including a complete treatment of charge-exchange effects. Since charge-exchange reactions are the dominant effect in neutral transport below about 10 eV, the temperatures below this value in our model are very uncertain. A separate investigation of these effects suggests, however, that charge exchange should not lead to a major increase in limiter sputtering.[15] Finally, we note that radiative losses from the plasma boundary depend sensitively on the distribution of electron and impurity density near the limiter. While the other features of our analytic model are relatively insensitive to its simplistic geometry, the total *radiative loss is only an order of magnitude estimate* without a detailed two-dimensional multispecies transport analysis. It is therefore possible that impurity radiation losses not included in our two-dimensional model could make a significant contribution to formation of a low temperature plasma near the limiter plate. It therefore seems reasonable, but not certain, that a solution exists with low plasma temperature near the limiter, but the exact plasma temperature which may be obtained is uncertain. The questions remain of whether our solutions are accessible and stable.

As to the question of accessibility, we find a continuum of solutions as the density is gradually raised. We therefore expect the high density solutions to be approached merely by reducing the pumpout rate. Only if the radial transport were increasing at higher density might one possibly expect a bifurcation, with low and high recycling solutions simultaneously possible at a given pumpout rate. (This may be the case in a divertor where neoclassical and/or charge-exchange effects can significantly affect radial transport at very high density.) In such a case, the high density solution would be obtained by temporarily reducing the pumpout rate or by depositing a fueling pellet in the scrapeoff. Next consider the question of stability. Since high density solutions are strongly influenced by volume losses, they tend to evolve towards even higher density until the temperature is too low to sustain further volume losses. The high density state should therefore be a thermally stable equilibrium. Provided the low temperature region near the limiter occupies a small fraction of the radial current profile, as in Fig. 2, it may not have a significant effect on stability of potentially disruptive low MHD mode numbers. More detailed analysis of solutions such as those presented here may therefore be fruitful.

ACKNOWLEDGMENTS

Useful conversations with F. Engelmann, K. Lackner, D. Heifetz, D. Post, G. Rewoldt, and J. Schmidt are gratefully acknowledged. We are particularly grateful to C. Boley for supplying poloidal flux plots from the WHIST code and the Max Planck Institut für Plasmaphysik for hosting much of this work.

This work was supported by the U.S. Department of Energy Contract No. DE-AC02-76-CHO-3073, and through the Euratom-FOM association agreement by ZWO and Euratom.

REFERENCES

[1]B.J. Braams, P. J. Harbour, M.F.A. Harrison, E. S. Hotston, and J. G. Morgan, J. Nucl. Mater. 121, 75-81 (1984).

[2]A. Gibson and M. L. Watkins, "Controlled Fusion and Plasma Physics," in Proceedings of the Eighth European Conference, Prague, 1977, Vol. 1, p. 31.

[3]M. L. Watkins, J. G. Cordey, A. E. P. M. Abels-van Maanen, J. E. C. Roberts, and P. M. Stubberfield, "Influence of Edge Plasma Models on JET Predictions," in Proceedings of the Ninth International Conference on Plasma Physics and Controlled Fusion Research, Baltimore, 1982, (IAEA, Vienna, 1983), Vol. 1, paper IAEA-CN-41/D-2-1.

[4]W. D. Langer and C. E. Singer, "Two-Chamber Model for Divertors with Plasma Recycling," Princeton Plasma Physics Laboratory Report No. PPPL-2160 (1984).

[5]P. J. Harbour and J. G. Morgan, "Models and Codes for the Plasma Edge Region," Culham Laboratory Report R234 (1982); P. J. Harbour, Nucl. Fusion (in press).

[6]S. I. Braginskii, in Reviews of Plasma Physics, edited by M. A. Leontovich, (Consultants Bureau, NY, 1965), Vol. 1, pp. 205-311.

[7]M. Keilhacker, K. Lackner, K. Behringer, H. Murmann, and H. Niedermeyer, Physica Scripta 71-72, 443 (1982).

[8]D. E. Post, R. V. Jensen, C. B. Tarter, W. H. Grasberger, and W. A. Lokke, At. Data Nucl. Data Tables 20, 397 (1977).

[9]B. J. Braams, "Modelling of a Transport Problem in Plasma Physcs," in Topics in Applied Numerical Analysis, J. G. Verwer, editor, (CWI Syllabus, Centrum voor Wiskunde en Informatica, Amsterdam, 1984).

[10]B. J. Braams, "Numerical Studies of the Two-Dimensional Scrape-off Plasma," in Proceedings of the Eleventh European Conference on Controlled Fusion and Plasma Physics, Aachen, 1983, EPS 7D, Part II, pp. 431-434.

[11] M. Petravic, D. Heifetz, and D. Post, "Modelling Analysis of Tokamaks with Divertors and Pumped Limiters," in Proceedings of the Tenth International Conference on Plasma Physics and Controlled Nuclear Fusion Research, London, 1984, paper IAEA-CN-44/E-II-5 (in press).

[12] C. E. Singer P. G. P. Seidl, D. E. Post, and P. H. Rutherford, J. Fusion Energy 1, 275 (1981).

[13] C. E. Singer, "An Assessment of Local Transport," Princeton Plasma Physics Laboratory, Applied Physics Division Report No. 31 (1984).

[14] C. E. Singer, J. Fusion Energy 3, 231 (1983).

[15] D. Heifetz, D. Post, M. Petravic, J. Weisheit, and G. Bateman, J. Comput. Phys. 46, 309 (1982).

FIGURE CAPTIONS

FIG. 1. Geometry for analytic and 2-d models of TFCX scrapeoff.

FIG. 2. (a) Electron density and (b) electron temperature projected onto TFCX geometry, for $\chi_e = 5 \times 10^4 cm^2/s$.

FIG. 3. Electron temperature in front of limiter tip (at first significant computational zone - zone 3) versus inner boundary density.

FIG. 4. Poloidal energy flux to limiter. θ is the inclination of the limiter to the poloidal flux contours (cf. Fig. 2). $P_{lim}/\cos\theta$ is the energy flux density in the poloidal direction. The largest limiter loading occurs at the limiter tip, where $\theta = 0$.

APPENDIX A: EQUATIONS FOR THE TWO-DIMENSIONAL MODEL

We employ a system of equations governing the ion density n_i, the parallel flow velocity $u_\parallel$, the radial diffusion velocity v, and electron- and ion temperatures T_e and T_i. Auxiliary physical quantities are the electron density, $n_e = Z_i n_i$, the mass density, $\rho = m_i n_i$, the total and partial pressures, $p = p_e + p_i = n_e T_e + n_i T_i$, and the poloidal flow velocity, $u = \frac{B_\theta}{B} u_\parallel$. The coordinates x and y correspond to the poloidal and radial directions respectively. $\sqrt{g}$, h_x, and h_y are metric coefficients; the coordinate system may be curvilinear, although it must be orthogonal. The equations are:

$$\frac{\partial}{\partial t} n_i + \frac{1}{\sqrt{g}} \frac{\partial}{\partial x}\left(\frac{\sqrt{g}}{h_x} n_i u\right) + \frac{1}{\sqrt{g}} \frac{\partial}{\partial y}\left(\frac{\sqrt{g}}{h_y} n_i v\right) = S_n \tag{A.1}$$

$$\begin{aligned}
&\frac{\partial}{\partial t}(\rho u_\parallel) + \frac{1}{\sqrt{g}} \frac{\partial}{\partial x}\left(\frac{\sqrt{g}}{h_x} \rho u u_\parallel - \frac{\sqrt{g}}{h_x^2} \eta_x^i \frac{\partial u_\parallel}{\partial x}\right) \\
&\quad + \frac{1}{\sqrt{g}} \frac{\partial}{\partial y}\left(\frac{\sqrt{g}}{h_y} \rho v u_\parallel - \frac{\sqrt{g}}{h_y^2} \eta_y^i \frac{\partial u_\parallel}{\partial y}\right) = S_{m u_\parallel} - \frac{B_\theta}{B} \frac{1}{h_x} \frac{\partial p}{\partial x}
\end{aligned} \tag{A.2}$$

$$v = -\frac{D}{h_y} \frac{\partial}{\partial y}(\ln n_i) \tag{A.3}$$

$$\begin{aligned}
&\frac{\partial}{\partial t}\left(\frac{3}{2} n_e T_e\right) + \frac{1}{\sqrt{g}} \frac{\partial}{\partial x}\left(\frac{\sqrt{g}}{h_x} \frac{5}{2} n_e u T_e - \frac{\sqrt{g}}{h_x^2} \kappa_x^e \frac{\partial T_e}{\partial x}\right) \\
&\quad + \frac{1}{\sqrt{g}} \frac{\partial}{\partial y}\left(\frac{\sqrt{g}}{h_y} \frac{5}{2} n_e v T_e - \frac{\sqrt{g}}{h_y^2} \kappa_y^e \frac{\partial T_e}{\partial y}\right) \\
&\quad = S_E^e - k(T_e - T_i) + \frac{u}{h_x} \frac{\partial p_e}{\partial x} + \frac{v}{h_y} \frac{\partial p_e}{\partial y}
\end{aligned} \tag{A.4}$$

$$\begin{aligned}
&\frac{\partial}{\partial t}\left(\frac{3}{2} n_i T_i + \frac{1}{2} \rho u_\parallel^2\right) \\
&\quad + \frac{1}{\sqrt{g}} \frac{\partial}{\partial x}\left(\frac{\sqrt{g}}{h_x}\left(\frac{5}{2} n_i u T_i + \frac{1}{2} \rho u u_\parallel^2\right) - \frac{\sqrt{g}}{h_x^2}\left(\kappa_x^i \frac{\partial T_i}{\partial x} + \frac{1}{2} \eta_x^i \frac{\partial u_\parallel^2}{\partial x}\right)\right) \\
&\quad + \frac{1}{\sqrt{g}} \frac{\partial}{\partial y}\left(\frac{\sqrt{g}}{h_y}\left(\frac{5}{2} n_i v T_i + \frac{1}{2} \rho v u_\parallel^2\right) - \frac{\sqrt{g}}{h_y^2}\left(\kappa_y^i \frac{\partial T_i}{\partial y} + \frac{1}{2} \eta_y^i \frac{\partial u_\parallel^2}{\partial y}\right)\right) \\
&\quad = S_E^i + k(T_e - T_i) - \frac{u}{h_x} \frac{\partial p_e}{\partial x} - \frac{v}{h_y} \frac{\partial p_e}{\partial y}
\end{aligned} \tag{A.5}$$

S_n, $S_{m u_\parallel}$, S_E^e, and S_E^i are volume sources of ions, momentum, electron, and ion energy. η_x^i and η_y^i are the poloidal and radial ion viscosity coefficients; $\kappa_x^{e,i}$ and $\kappa_y^{e,i}$ are thermal conductivities. The poloidal coefficients are related to classical parallel coefficients according to $\eta_x^i = B_\theta^2/B^2 \cdot \eta_\parallel^i$, and similarly for $\kappa_x^{e,i}$. The radial coefficients, including D, are anomalous. $k(T_e - T_i)$ is the electron-ion energy equilibration term, and the ∇p_e term on the right-hand side of the energy equations represents work done by the electric field.

#84P0223

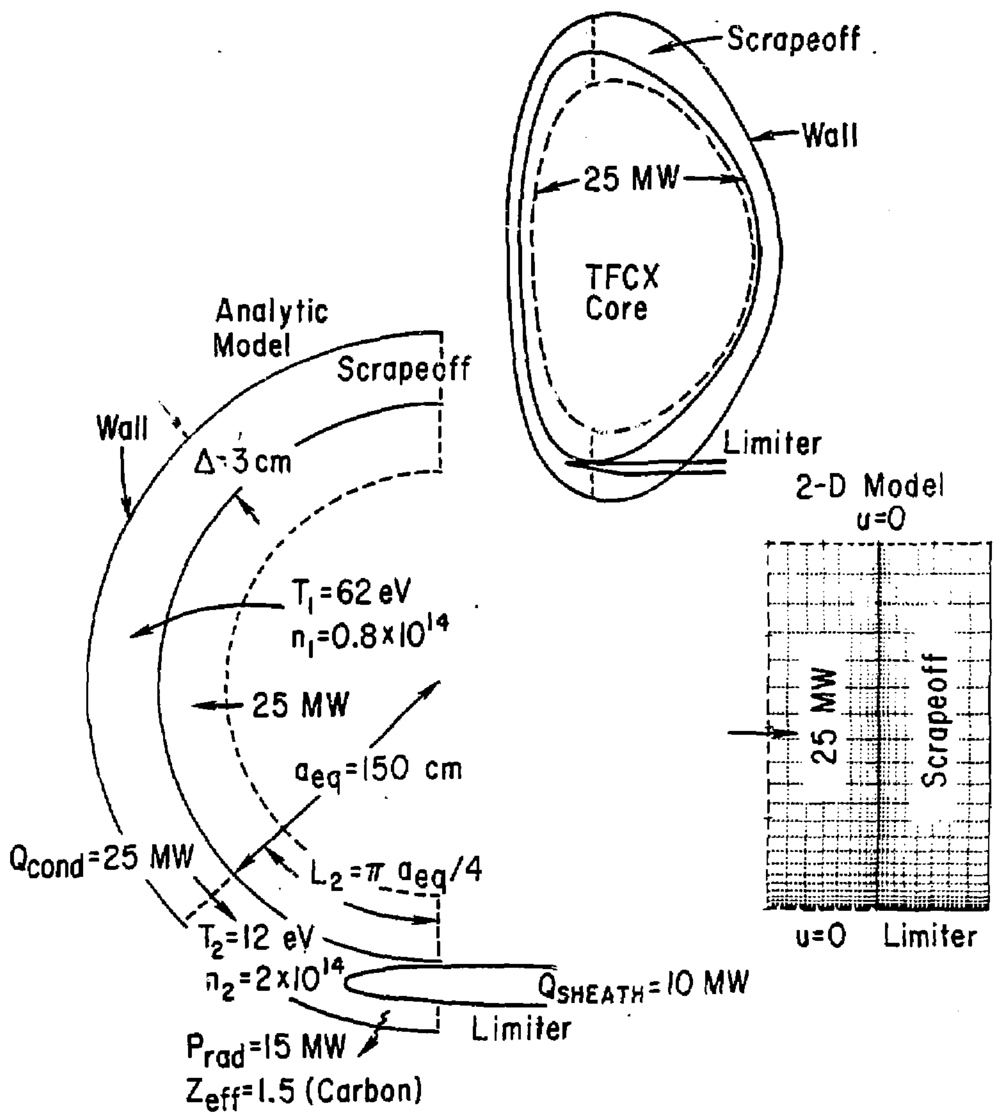

FIG. 1

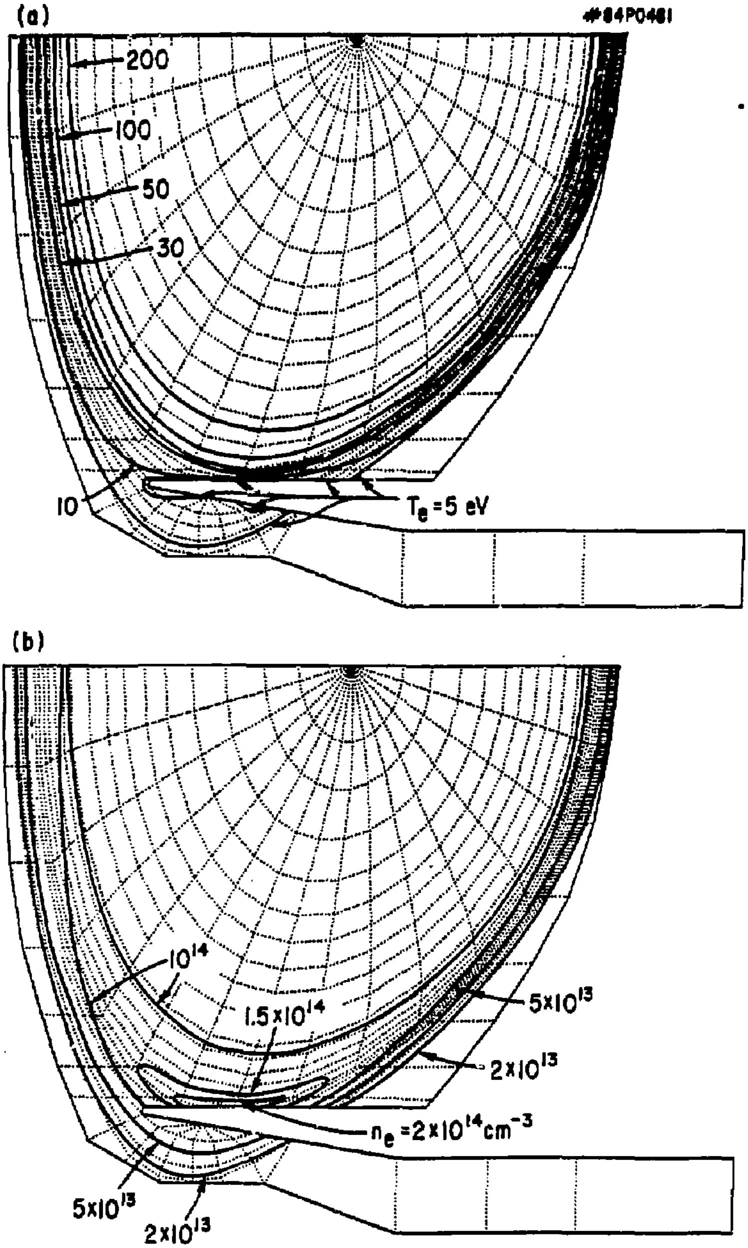
(a)
#84P0481
200
100
50
30
10
T_e =5 eV
(b)
10^{14}
1.5×10^{14}
5×10^{13}
2×10^{13}
$n_e = 2\times10^{14}$ cm^{-3}
5×10^{13}
2×10^{13}

FIG. 2

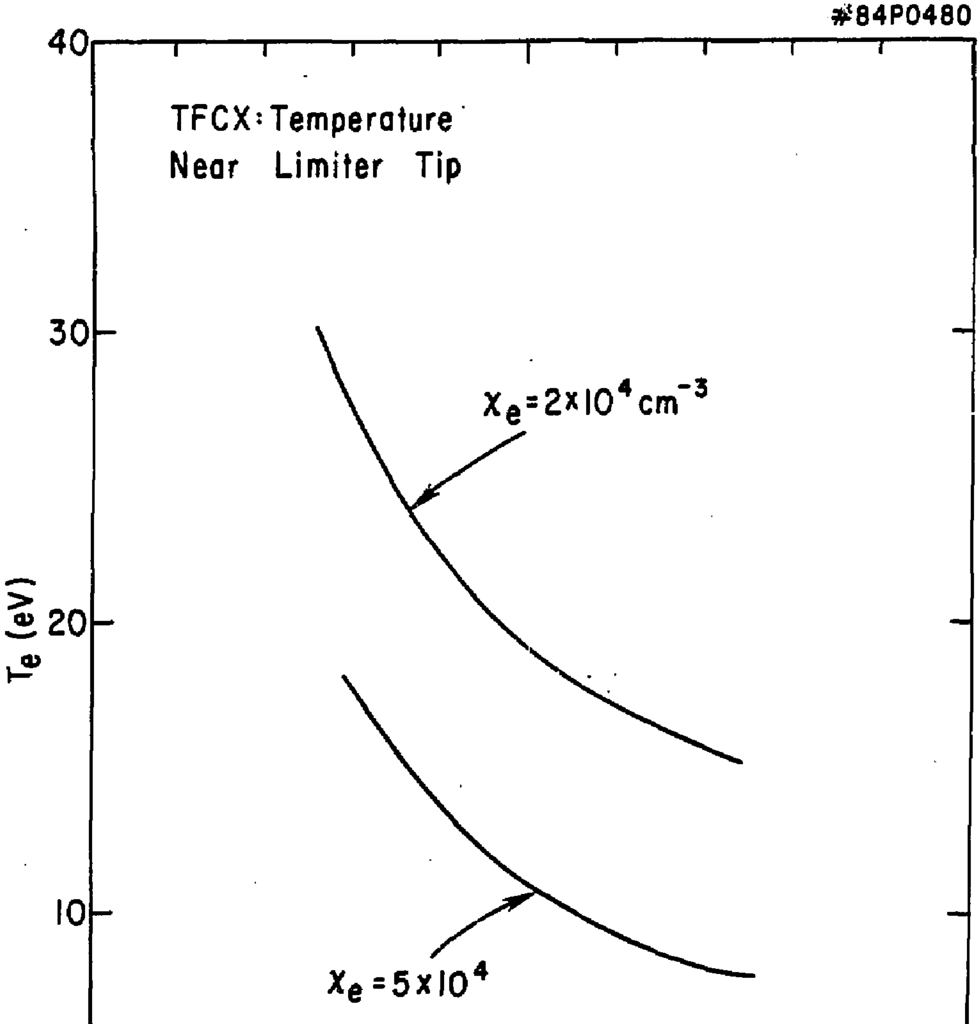
#84P0480
TFCX: Temperature
Near Limiter Tip
$\chi_e = 2 \times 10^4 \, cm^{-3}$
$\chi_e = 5 \times 10^4$
T_e (eV)
40
30
20
10
0
0
1
2
$n_{e,CORE}$ ($10^{14} cm^{-3}$)

FIG. 3

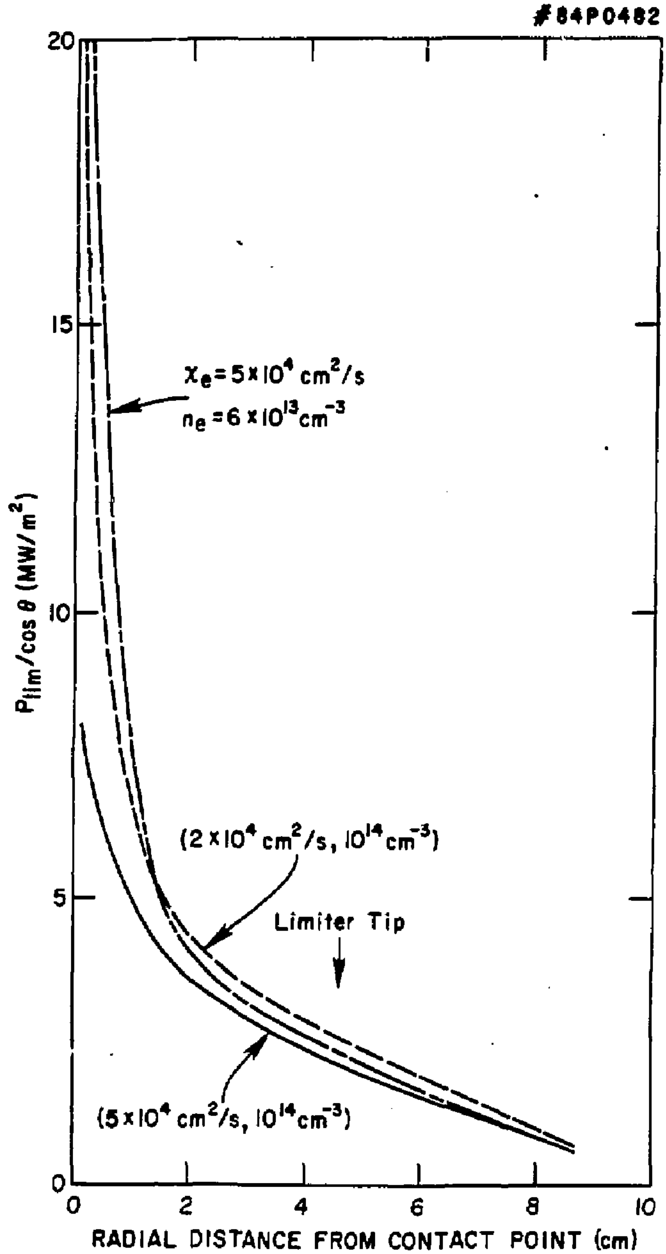
#84P0482
$P_{lim}/\cos\theta$ (MW/m^2)
$\chi_e = 5\times10^4$ cm^2/s
$n_e = 6\times10^{13}$ cm^{-3}
(2×10^4 cm^2/s, 10^{14} cm^{-3})
Limiter Tip
(5×10^4 cm^2/s, 10^{14} cm^{-3})
RADIAL DISTANCE FROM CONTACT POINT (cm)
0
5
10
15
20
0
2
4
6
8
10

FIG. 4

EXTERNAL DISTRIBUTION IN ADDITION TO UC-20

Plasma Res Lab, Austra Nat'l Univ, AUSTRALIA
Dr. Frank J. Paoloni, Univ of Wollongong, AUSTRALIA
Prof. I.R. Jones, Flinders Univ., AUSTRALIA
Prof. M.H. Brennan, Univ Sydney, AUSTRALIA
Prof. F. Cap, Inst Theo Phys, AUSTRIA
Prof. Frank Verheest, Inst theoretische, BELGIUM
Dr. D. Palumbo, Dg XII Fusion Prog, BELGIUM
Ecole Royale Militaire, Lab de Phys Plasmas, BELGIUM
Dr. P.H. Sakanaka, Univ Estadual, BRAZIL
Dr. C.R. James, Univ of Alberta, CANADA
Prof. J. Teichmann, Univ of Montreal, CANADA
Dr. H.M. Skarsgard, Univ of Saskatchewan, CANADA
Prof. S.R. Sreenivasan, University of Calgary, CANADA
Prof. Tudor W. Johnston, INRS-Energie, CANADA
Dr. Hannes Barnard, Univ British Columbia, CANADA
Dr. M.P. Bachynski, MPB Technologies, Inc., CANADA
Chalk River, Nucl Lab, CANADA
Zhengwu Li, SW Inst Physics, CHINA
Library, Tsing Hua University, CHINA
Librarian, Institute of Physics, CHINA
Inst Plasma Phys, Academia Sinica, CHINA
Dr. Peter Lukac, Komenskeho Univ, CZECHOSLOVAKIA
The Librarian, Culham Laboratory, ENGLAND
Prof. Schatzman, Observatoire de Nice, FRANCE
J. Radet, CEN-BP6, FRANCE
AM Dupas Library, AM Dupas Library, FRANCE
Dr. Tom Mual, Academy Bibliographic, HONG KONG
Preprint Library, Cent Res Inst Phys, HUNGARY
Dr. S.K. Trehan, Panjab University, INDIA
Dr. Indra Mohan Lal Das, Banaras Hindu Univ, INDIA
Dr. L.K. Chavda, South Gujarat Univ, INDIA
Dr. R.K. Chhajlani, Vikram Univ. INDIA
Dr. B. Dasgupta, Saha Inst, INDIA
Dr. P. Kaw, Physical Research Lab, INDIA
Dr. Phillip Rosenau, Israel Inst Tech, ISRAEL
Prof. S. Cuperman, Tel Aviv University, ISRAEL
Prof. G. Rostagni, Univ Di Padova, ITALY
Librarian, Int'l Ctr Theo Phys, ITALY
Miss Clelia De Palo, Assoc EURATOM-ENEA, ITALY
Biblioteca, del CNR EURATOM, ITALY
Dr. H. Yamato, Toshiba Res & Dev, JAPAN
Direc. Dept. Lg. Tokamak Dev. JAERI, JAPAN
Prof. Nobuyuki Inoue, University of Tokyo, JAPAN
Research Info Center, Nagoya University, JAPAN
Prof. Kyoji Nishikawa, Univ of Hiroshima, JAPAN
Prof. Sigeru Mori, JAERI, JAPAN
Library, Kyoto University, JAPAN
Prof. Ichiro Kawakami, Nihon Univ, JAPAN
Prof. Satoshi Itoh, Kyushu University, JAPAN
Dr. D.I. Choi, Adv. Inst Sci & Tech, KOREA
Tech Info Division, KAERI, KOREA
Bibliotheek, Fom-Inst Voor Plasma, NETHERLANDS
Prof. B.S. Liley, University of Waikato, NEW ZEALAND
Prof. J.A.C. Cabral, Inst Superior Tecn, PORTUGAL
Dr. Octavian Petrus, ALI CUZA University, ROMANIA
Prof. M.A. Hellberg, University of Natal, SO AFRICA
Dr. Johan de Villiers, Plasma Physics, Nucor, SO AFRICA
Fusion Div. Library, JEN, SPAIN
Prof. Hans Wilhelmson, Chalmers Univ Tech, SWEDEN
Dr. Lennart Stenflo, University of UMEA, SWEDEN
Library, Royal Inst Tech, SWEDEN
Centre de Recherchesen, Ecole Polytech Fed, SWITZERLAND
Dr. V.T. Tolok, Kharkov Phys Tech Ins, USSR
Dr. D.D. Ryutov, Siberian Acad Sci, USSR
Dr. G.A. Eliseev, Kurchatov Institute, USSR
Dr. V.A. Glukhikh, Inst Electro-Physical, USSR
Institute Gen. Physics, USSR
Prof. T.J.M. Boyd, Univ College N Wales, WALES
Dr. K. Schindler, Ruhr Universitat, W. GERMANY
Nuclear Res Estab, Julich Ltd, W. GERMANY
Librarian, Max-Planck Institut, W. GERMANY
Bibliothek, Inst Plasmaforschung, W. GERMANY
Prof. R.K. Janev, Inst Phys, YUGOSLAVIA